Transformation and stable isotope fractionation of the urban biocide terbutryn during biodegradation, photodegradation and abiotic hydrolysis

Tobias Junginger, Sylvain Payraudeau, Gwenaël Imfeld

Transformation and stable isotope fractionation of the urban biocide terbutryn during biodegradation, photodegradation and abiotic hydrolysis

Tobias Junginger, Sylvain Payraudeau and Gwenaël Imfeld*

Institut Terre et Environnement de Strasbourg (ITES), Université de Strasbourg/ EOST/ ENGEES, CNRS UMR 7063, F-67084 Strasbourg, France

*Corresponding author: G. Imfeld, Phone: +33 3 6885 0474, Email: imfeld@unistra.fr

Manuscript for Chemosphere

Graphical abstract

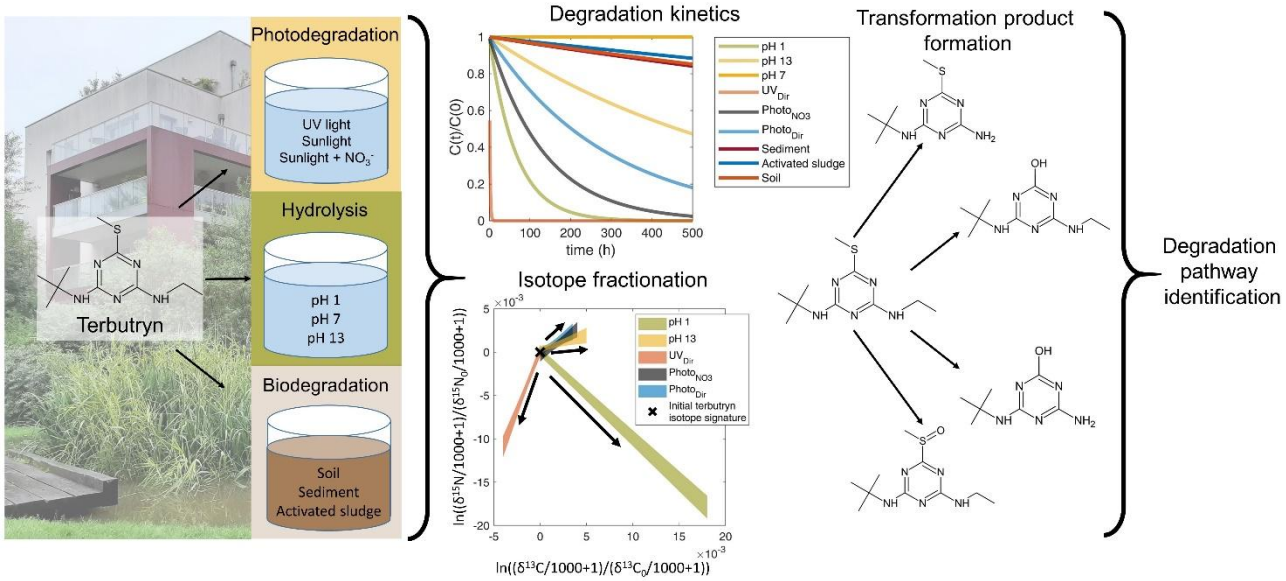

Highlights

- The biocide terbutryn released from building facades can contaminate soil and water
- Laboratory microcosms to examine terbutryn hydrolysis, photo- and bio-degradation
- Terbutryn degradation half-lives are high under environmental conditions
- Transformation products and CSIA of terbutryn to identify degradation pathways
- Differentiation of terbutryn degradation pathways based on dual-isotope values ($\Lambda^{N/C}$)

Abstract

Terbutryn is a widely used biocide in construction materials like paint and render to prevent the growth of microorganisms, algae and fungi. Terbutryn is released from the facades into the environment during rainfall, contaminating surface waters, soil and groundwater. Knowledge of terbutryn dissipation from the facades to aquatic ecosystems is scarce. Here, we examined in laboratory microcosms degradation half-lives, formation of transformation products and carbon and nitrogen isotope fractionation during terbutryn direct (UV light with λ = 254 nm and simulated sunlight) and indirect (simulated sunlight with nitrate) photodegradation, abiotic hydrolysis (pH = 1, 7 and 13), and aerobic biodegradation (stormwater pond sediment, soil and activated sludge). Biodegradation half-lives of terbutryn were high (>80 d). Photodegradation under simulated sunlight and hydrolysis at extreme pH values indicated slow degradability and accumulation in the environment. Photodegradation resulted in a variety of transformation products, whereas abiotic hydrolysis lead solely to terbutryn-2-hydroxy in acidic and basic conditions. Biodegradation indicates degradation to terbutryn-2-hydroxy through terbutryn-sulfoxide. Compound-specific isotope analysis (CSIA) of terbutryn holds potential to differentiate degradation pathways. Carbon isotope fractionation values (ε_C) ranged from −3.4 ± 0.3 ‰ (hydrolysis pH 1) to +0.8 ± 0.1 ‰ (photodegradation under UV light), while nitrogen isotope fractionation values ranged from −1.0 ± 0.4 ‰ (simulated sunlight photodegradation with nitrate) to +3.4 ± 0.2 ‰ (hydrolysis at pH 1). In contrast, isotope fractionation during biodegradation was insignificant. $\Lambda^{N/C}$ values ranged from −1.0 ± 0.1 (hydrolysis at pH 1) to 2.8 ± 0.3 (photodegradation under UV light), allowing to differentiate degradation pathways. Combining the formation of transformation products and stable isotope fractionation enabled identifying distinct degradation pathways. Altogether, this study highlights the potential of CSIA to follow terbutryn degradation *in situ*

and differentiate prevailing degradation pathways, which may help to monitor urban biocide remediation and mitigation strategies.

Keywords: CSIA; Terbutryn; Hydrolysis; Photodegradation; Biodegradation; Transformation products

1. Introduction

Biocides are added as in-can and film preservatives in building materials to prevent algae and microbial growth on facade materials like paints and renders. During rainfall events, biocides and their transformation products (TPs) are washed out from building materials and enter into the environment (Bollmann et al., 2016; Burkhardt et al., 2012; Linke et al., 2021; Schoknecht et al., 2009; Wittmer et al., 2011). Lab-scale experiments have demonstrated the export of urban biocides from silicone render, acrylate render, roof paint and facade paints (Burkhardt et al., 2012; Jungnickel et al., 2008; Schoknecht et al., 2009; Styszko et al., 2015). However, knowledge of the contribution of dissipation processes controlling the reactive transport of urban biocides from facades to surface waters, soil and groundwater remains scarce.

Among urban biocides, an active compound of major concern is terbutryn, acting as a photosynthesis inhibitor (Jurado et al., 2011). Terbutryn is still used as a pre-emergent or post-emergent herbicide in agriculture in several countries (Carazo-Rojas et al., 2018; LeBaron et al., 2008). In the EU, terbutryn is prohibited for agricultural applications since 2003 (European Council Directive 91/414/EEC, 2002) and is defined as a priority substance since 2013 according to the Water Framework Directive (WFD) (European Council Directive 2013/39/EU, 2013). Terbutryn, measured in concentrations up to 5.6 μg L^{-1} in German rivers exceeds predicted no-effect concentrations (PNEC, 0.003 to 0.034 μg L^{-1}) (Burkhardt et al.,

2009; Kresmann et al., 2018; Quednow and Püttmann, 2007) and is detected in groundwater (Hensen et al., 2018). The redundant detection of terbutryn in waters may be related to its low removal in wastewater treatment plants (WWTP) (Luft et al., 2014; Paijens et al., 2021). Altogether, this emphasizes significant, and possibly ecotoxic, release of terbutryn into surface water. However, the contribution of degradative processes (i.e., photodegradation, hydrolysis and biodegradation) and non-degradative process (i.e., sorption and dilution) to the overall dissipation of terbutryn and its TPs is largely unknown.

Photodegradation may either occur directly on the facades or in water bodies, such as retention ponds or rivers (Bollmann et al., 2016; Minelgaite et al., 2017; Sakkas et al., 2006; Urbanczyk et al., 2019). Direct photodegradation refers to the absorption of light by a molecule leading to bond cleavage, whereas indirect photodegradation results from the excitation of other molecules, e.g. nitrate or dissolved organic carbon (DOC), and the formation of radical reactive species mediating bond cleavages (Schwarzenbach et al., 2005). Terbutryn degrades in the range of sunlight wavelengths (Hensen et al., 2019), although degradation is slow under environmental conditions (Minelgaite et al., 2017). Terbutryn photodegradation occurred in paint and on facades under controlled laboratory conditions and in the environment (Bollmann et al., 2016; Schoknecht et al., 2021; Urbanczyk et al., 2019). Several TPs of terbutryn have been identified under irradiation with UV light (Hensen et al., 2018) and under simulated sunlight during direct and indirect photodegradation in aqueous solutions and on paint surfaces (Hensen et al., 2019; Urbanczyk et al., 2019). This raises the issue of the formation of photodegradation TPs and their release from facades.

Hydrolysis is a major pathway of pesticide degradation, which can be abiotically or biologically-mediated (Fenner et al., 2013), depending on pH and temperature (Mabey and Mill, 1978). Some studies indicate only minor abiotic hydrolysis of other triazine pesticides,

such as atrazine, under moderate acidic or alkaline pHs and degradation mainly occurring at extreme pHs (<4 or >12) (Masbou et al., 2018; Meyer et al., 2009; Torrentó et al., 2021).

Biodegradation of terbutryn may occur in soils collecting runoff from facades, in WWTPs and in water bodies receiving discharges from separated sewers. Biodegradation half-lives of terbutryn in laboratory soil microcosms ranged from 7 (32 °C, 10 % soil moisture content) to 227 days (4°C with 10 % soil moisture content) (Lechón et al., 1997), and from 180 to 240 days in water with river sediment under aerobic conditions (Muir and Yarechewski, 1982), and up to 650 days under anaerobic conditions (Talja et al., 2008). Biodegradation in activated WWTP sludge resulted mainly in the formation of terbutryn-sulfoxide (TerSO). TerSO was further degraded to the hydroxy-derivate terbutryn-2-hydroxy (TerOH) under acidic conditions (Luft et al., 2014). TerSO prevailed in the early state of degradation under aerobic soil biodegradation experiments, with declining concentrations throughout the experiment. TerOH, desbutyl-2-hydroxy-terbutryn (TerDesBOH) and desethyl-terbutryn (TerDesE) were gradually formed, with minor contribution of desethyl-2-hydroxy-terbutryn (TerDesEOH) (Bollmann et al., 2017a). Although the occurrence of TPs in the environment indicates terbutryn degradation, further TP degradation, sorption or dilution may limit the identification and the quantification of specific transformation pathways.

In this context, following up changes of the stable isotope composition (natural isotope abundance) of the residual, non-degraded fraction of a pollutant may help to evaluate degradation without considering concentration data of parent compound or TPs (Alvarez-Zaldívar et al., 2018; Elsner et al., 2012; Elsner and Imfeld, 2016; Schmidt et al., 2004). Typically, light isotopes (e.g., ^{12}C) need a lower activation energy for bond cleavage compared to heavy isotopes (e.g., ^{13}C), resulting in faster reaction times and enrichment of heavy isotopologues in the non-degraded fraction (Elsner, 2010). In contrast, non-degradative processes like sorption, dilution or advection generally cause insignificant isotope

fractionation (Höhener and Yu, 2012; Schüth et al., 2003). In particular, compound-specific isotope analysis (CSIA) of pollutants may help to identify reaction pathways by measuring changes in stable isotope ratios (e.g., $^{13}C/^{12}C$, $^{15}N/^{14}N$), which are often reaction-specific (Alvarez-Zaldívar et al., 2018; Elsner, 2010; Elsner and Imfeld, 2016; Fischer et al., 2016; Meyer et al., 2009; Torrentó et al., 2021). In some cases, changes in isotope ratios may be related to the extent of degradation using isotope fractionation values (ε) that are typically retrieved from laboratory experiments under controlled conditions (Coplen, 2011; Hoefs, 2015). While CSIA has been used to study transformation of similar triazine type herbicides, such as atrazine and ametryn (Drouin et al., 2021; Hartenbach et al., 2008; Lihl et al., 2020; Masbou et al., 2018; Meyer et al., 2009; Schürner et al., 2015; Torrentó et al., 2021), isotope fractionation of terbutryn during degradation has not been examined yet.

The purpose of this study was to examine the degradation rates and stable isotope fractionation during abiotic hydrolysis, biodegradation and photodegradation of terbutryn to improve the interpretation of terbutryn degradation from the facades to sink ecosystems, such as soil and groundwater, in urban settings. Different terbutryn degradation pathways may lead to distinct patterns of TP formation and stable isotope fractionation. We thus examined the reaction kinetic rate constants, the TP formation, and carbon and nitrogen CSIA data to evaluate degradation pathways of terbutryn and the potential of CSIA to follow up terbutryn degradation *in situ* and distinguish degradation processes.

2. Material & Methods

2.1. Chemicals

Solvents (dichloromethane (DCM) and n-Pentane) were HPLC-grade (>99.9 %) and purchased from Sigma-Aldrich (St. Louis, MO, USE). Analytical standards with purity >98% (terbutryn and alachlor D-13) were purchased from PESTANAL (St. Louis, MO, USA).

Standards of terbutryn TPs TerOH, TerDesE and TerDesEOH (purity >98 %) were purchased from HPC Standards GmbH (Borsdorf, Germany), TerSO (purity >97%) was purchased from MicroCombiChem GmbH (Wiesbaden, Germany). Water, acetonitrile and formic acid for analysis with HPLC-MS were LC/MS grade (Biosolve, France). Buffer solutions were prepared using DI-water (>18 MΩ), hydrochloric acid (37 %, AnalaR NORMAPUR), potassium phosphate monobasic (>99.5 %, Sigma Aldrich), potassium chloride (>99.5 %, VWR Chemicals BDH) and sodium hydroxide (>95 %, Sigma Aldrich). Nitrate solutions for photodegradation experiments were prepared with calcium nitrate tetrahydrate (>99 %, Sigma Aldrich).

2.2. Experimental setup

Photodegradation experiment. Photodegradation experiments in aqueous solutions were conducted under UV irradiation (UV_{Dir}), under simulated sunlight in pure water ($Photo_{Dir}$) and under simulated sunlight with 20 mg L^{-1} nitrate ($Photo_{NO3}$) to mimic environmental conditions in surface waters. UV_{Dir} was conducted using a temperature-controlled black box with a low-pressure mercury lamp (Philipps, TUV 6W G6T5) providing a single-band light at $\lambda = 254$ nm. Simulated sunlight was replicated using a QSUN XE-1 test chamber (Q-LAB, Westlake, OH USA) with a xenon arc lamp and a daylight-Q filter with a nominal cut-on at 295 nm. The irradiation intensity was set to 0.68 W/m²/nm at 340 nm which matches best with maximum solar irradiation and represents an intensity of ≈1200 W/m² integrated over all wavelengths (QSun/QLab, 2011). Initial terbutryn concentrations were 10 mg L^{-1} in the aqueous solutions. Three independent beakers (50 mL beakers containing 40 mL solution) for sacrificial sampling were prepared for each sampling. Additionally, dark controls and process blanks were prepared for three successive samplings throughout the experiment. Sample preparation and sampling are detailed in Table S1. The pH of aqueous solutions

containing mixtures of terbutryn and TPs in different proportion and in the relevant concentration range (1 – 10 mg L^{-1}), with and without calcium nitrate tetrahydrate ($Ca(NO_3)_2 \cdot 4\ H_2O$), did not change significantly (7.0 ± 0.5) (Section SI 2.2).

Hydrolysis experiment. Hydrolysis experiments were carried out in triplicate in 400 mL Schott glass bottles under dark and sterile conditions. Three aqueous buffer solutions were prepared with sterilized DI water at pH = 1, 7 and 13 and sterilized by filtration through sterile 0.2 µm PTFE filters (Rotilabo®, Carl Roth®, France). Extreme pH values were chosen to increase degradation kinetics and study reaction pathways and associated isotope fractionation. Buffer solutions were spiked with terbutryn to a final concentration of 10 mg L^{-1}. Additional process blanks without terbutryn were prepared for each pH and sampled three times throughout the experiment. Solutions were incubated at 60 °C to accelerate the reaction. The preparation of buffer solutions, sample preparation and sampling procedures are detailed in Table S1 and S2.

Biodegradation. Terbutryn biodegradation in different systems exposed to biocide effluent was examined in microcosm experiments: (i) water from stormwater retention pond with 100 mg L^{-1} of 2 mm-sieved pond sediment (PondSed), (ii) soil from a stormwater swale system (soil) and (iii) activated sludge from WWTP diluted 1:10 (v:v) in milliQ water. Composite samples (n>5 subsamples) of either soil, pond water or sediment exposed to facade runoff through drainage pipes and surface flow were collected in the Aldelshoffen district in Schiltigheim (Strasbourg Eurometropolis, Bas-Rhin, France) and the respective samples were mixed together thoroughly. The activated sludge was collected in the main WWTPs of Strasbourg, receiving diluted urban runoff through combined sewer systems. The frequent exposure of sediment, soil and activated sludge to terbutryn from facade runoff may lead to microbial adaptation and favor terbutryn biodegradation (Poursat et al., 2019; Spain et al.,

1980). The collection procedure and physico-chemical characteristics of the samples used in the biodegradation experiments are detailed in the SI.

Aerobic biodegradation microcosms consisted in 50 mL vials crimped with butyl/PTFE caps filled either with 30 mL of spiked stormwater retention pond water with sediment, 30 mL spiked diluted sewage sludge or 5 g of spiked soil. A needle with a 0.2 µm syringe filter was stuck through the cap to maintain oxic conditions without water loss (Torabi et al., 2020). For each soil sample, 5 g of soil were spiked with terbutryn, to reach a final concentration of 120 µg g^{-1}, adjusted to a water content of 40 % and thoroughly mixed. Concentrations are representative for accumulation of terbutryn on small receiving surfaces exposed to repeated facade runoff with emission rates of several mg m^{-2} $event^{-1}$ (Bollmann et al., 2017b, 2016; Burkhardt et al., 2012). Stormwater retention pond and activated sludge samples were spiked with terbutryn at 10 mg L^{-1} and divided into the different microcosms for sacrificial sampling. Concentrations are representative for direct facade runoff from new buildings (Bollmann et al., 2017b, 2016; Burkhardt et al., 2012). Process blanks without terbutryn and sterile controls were prepared for all setups. Microcosms were incubated at room temperature (21 °C) and constantly shaken on an orbital shaker at 120 rpm. During each sampling time (Table S1), triplicate microcosms were retrieved for extraction and analysis.

2.3. Terbutryn extraction and quantification

Liquid samples were extracted using liquid-liquid extraction. Briefly, the entire sample for biodegradation experiments and 30 mL for photodegradation experiments were transferred into 40 mL amber glass vials and terbutryn was extracted with DCM (3 mL). Samples were shaken (600 rpm) for 5 min, ultrasonicated for 15 min, shaken again for 5 seconds and centrifuged at 1500 rpm for 5 min. Solvent was recovered and the whole procedure was repeated three times. The extracts were pooled and evaporated under gentle N_2 stream. Samples were resuspended in 0.5 mL DCM. Soil samples followed a modified solid-

liquid extraction with 3:1 Pentane:DCM (v:v) and purification procedure (Droz et al., 2021; Ivdra et al., 2014). Water subsamples (1 mL) were collected at different time points and filtered at 0.2 µm for TP analysis (Table S1 and sections SI 1.2 – SI 1.4). All samples were stored in the freezer at –20°C until analysis. Recoveries of extraction methods and validation for CSIA (i.e., absence of stable isotope fractionation associated with the methods) are provided in SI (Section 1.5).

Terbutryn and four main TPs TerSO, TerOH, TerDesE and TerDesEOH (Table S5) were quantified using ultra high-pressure liquid chromatography (UHPLC) (Dionex/ Thermo Scientific UltiMate Dionex 3000) coupled to a triple quadrupole mass spectrometer (Thermo Scientific TSQ Quantiva), using a C18 column (Accucore 100 x 2.1, particle size 2.6 µm). Solvent gradients, mass transitions, LOQ and LOD are provided in SI (Table S6 and S7).

2.4. Compound-specific isotope analysis

Carbon and nitrogen stable isotope analysis was conducted using a GC/IRMS system consisting of a gas chromatograph (GC, TRACE Ultra ThermoFisher Scientific) coupled to an isotope ratio mass spectrometer (IRMS, DeltaV plus, ThermoFisher Scientific) via a GC combustion interface (IsoLink/Conflow IV, ThermoFisher Scientific) equipped with a TG-5MS column (60 m × 0.25 mm ID, 0.25 µm film thickness). The samples (0.3 - 3 µL) were injected via a split/splitless injector at 250 °C with helium as carrier gas at a 1.5 mL min^{-1} flow rate. The GC temperature program and quality controls are described in Section S1.9. $\delta^{13}C$ and $\delta^{15}N$ values were calibrated against the VPDB and air standards, respectively, using international reference materials AIEA600, USGS40 and USGS41. The range of the GC–IRMS where isotope values are independent of signal intensity for $\delta^{13}C$ and $\delta^{15}N$ values (i.e., the range of injected amount of terbutryn for which carbon and nitrogen isotope values are within a ± 0.5 ‰ interval) was established for peak amplitudes from 220 to 2560 for $\delta^{13}C$ (m/z = 44), and from 220 to 1480 for $\delta^{15}N$ (m/z = 28) (Figure S2).

2.5. Data analysis

For all degradation experiments, concentrations were plotted against experimental time and fitted using first order degradation kinetics with Matlab R2020 b using the fit function.

Isotope ratios were normalized to VPDB and air standards for carbon and nitrogen stable isotopes respectively and written in the delta notation (Elsner, 2010):

$$\delta_{sample}E\ [‰] = \left(\frac{R_{sample}}{R_{standard}} - 1\right) \cdot 1000$$

The Rayleigh equation was used to calculate the isotope values of the residual (non-degraded) fraction of terbutryn (Elsner, 2010):

$$ln\left(\frac{R_{t,E}}{R_{0,E}}\right) = ln\left(\frac{C_{t,E}}{C_{0,E}}\right) \cdot \frac{\varepsilon^{E}_{bulk}}{1000}$$

Where $R_{t,E}$ / $R_{0,E}$ is the isotope ratio of the element E (e.g. $^{13}C/^{12}C$ or $^{15}N/^{14}N$), $C_{t,E}$ and $C_{0,E}$ are concentrations of terbutryn at a specific time t and at the start of the experiment (0) and ε^{E}_{bulk} is the apparent isotope fractionation value. Apparent isotope values were derived from linear regression by taking into account each of the triplicate microcosms/samples individually (Scott et al., 2004). Given uncertainties correspond to the 95 % confidence interval (CI) of the slope of the linear regression. $\Lambda^{N/C}$ values were derived using the York regression, accounting for uncertainties in C and N isotope measurements (Höhener and Imfeld, 2021; Ojeda et al., 2019) according to:

$$\Lambda^{N/C} = \frac{\ln\left[\left(\frac{\delta^{15}N_t}{1000} + 1\right)/\left(\frac{\delta^{15}N_0}{1000} + 1\right)\right]}{\ln\left[\left(\frac{\delta^{13}C_t}{1000} + 1\right)/\left(\frac{\delta^{13}C_0}{1000} + 1\right)\right]}$$

For analysis of $\Lambda^{N/C}$ values, the R package IsoplotR was used (Vermeesch, 2018).

3. Results

3.1. Terbutryn photodegradation

Terbutryn photodegradation was faster under UV light than under simulated sunlight (Table 1), due to the absorption spectrum of terbutryn and irradiation intensity (Bollmann et al., 2016; Hensen et al., 2019; Minelgaite et al., 2017). Slower terbutryn degradation under simulated sunlight likely reflects the slight overlap of the absorption spectrum of terbutryn with simulated sunlight at wavelengths 290 – 300 nm (SI, Figure S4). Selecting a representative irradiation source, such as a filtered Xenon arc lamp, is thus crucial to infer environmentally relevant photodegradation kinetics, especially for compounds weakly absorbing sunlight, such as terbutryn (Hensen et al., 2019).

Table 1. Terbutryn degradation half-life ($t_{1/2}$) and degradation rate constant (k), isotope fractionation values for carbon (ε_C) and nitrogen (ε_N) and $\Lambda^{N/C}$ values. Uncertainties are given as 95% confidence interval (± 95% CI). NS: non-significant degradation or isotope fractionation ($\Delta\delta^{13}C$ or $\Delta\delta^{15}N$ <0.5 ‰ in biodegradation experiments).

	Degradation process	**$t_{1/2}$**	**k [s^{-1}]**	**ε_C [‰]**	**ε_N [‰]**	**$\Lambda^{N/C}$**
UV_{Dir}	Photodegradation	68.7 ± 24.6 min	$1.7\times10^{-4}\pm 9.4\times10^{-5}$	+0.8 ± 0.1	+2.2 ± 0.3	2.8 ± 0.3
$Photo_{NO3}$		93.6 ± 37.2 h	$2.1\times10^{-6}\pm 1.4\times10^{-6}$	–0.6 ± 0.2	–1.0 ± 0.4	0.8 ± 0.1
$Photo_{Dir}$		202.3 ± 83.3 h	$9.5\times10^{-7}\pm 6.7\times10^{-7}$	–0.7 ± 0.3	–0.5 ± 0.3	0.7 ± 0.2

pH 1	Abiotic Hydrolysis	45.4 ± 15.2 h	$4.2\times10^{-6} \pm 2.1\times10^{-6}$	–3.4 ± 0.3	+3.4 ± 0.2	–1.0 ± 0.1
pH 7		NS	NS	NS	NS	NS
pH 13		462.3 ± 173.3 h	$4.2\times10^{-7} \pm 2.5\times10^{-7}$	–1.3 ± 0.2	–0.4 ± 0.3	0.3 ± 0.1
Pond + sediment	Biodegradation	83.6 ± 27.6 d	$9.6\text{x}10^{-8} \pm 4.7\text{x}10^{-8}$	NS	NS	NS
Soil		90.2 ± 34.5 d	$8.9\text{x}10^{-8} \pm 5.5\text{x}10^{-8}$	NS	NS	NS
Activated sludge		117.1 ± 34.4 d	$6.9\text{x}10^{-8} \pm 2.9\text{x}10^{-8}$	NS	NS	NS

Photodegradation rate constants were twice higher with than without nitrate (Table 1). Nitrate concentrations are often above 20 mg/L in agricultural surface waters as well as effluents of WWTPs, where urban biocides are present as well. Irradiation of nitrate may form hydroxy radicals ($NO_3^- + H_2O \xrightarrow{h\nu} NO_2 + OH\cdot + OH$) acting as photocatalyst during indirect photodegradation of terbutryn (Schwarzenbach et al., 2005). Hence, terbutryn degradation rate constants increase with increasing formation of hydroxy radicals (Hensen et al., 2019; Lam et al., 2003). It is worth mentioning, that direct and indirect photodegradation can co-occur in water, limiting the estimation of the contribution of nitrate-mediated degradation. Direct and indirect terbutryn photodegradation may also already occur on facades (Bollmann et al., 2016; Schoknecht et al., 2021; Urbanczyk et al., 2019) then in sink aquatic ecosystems, including storm water retention systems (swale systems), rivers and lakes where terbutryn was frequently detected (Ccanccapa et al., 2016; Linke et al., 2021; Machate et al., 2021; Quednow and Püttmann, 2007). Besides nitrate, other substances (e.g. humic acids or dissolved organic matter) can catalyze photodegradation by providing radicals or decelerate photodegradation through absorption and shielding of the contaminant (Drouin et al., 2021; Wu et al., 2021; Zhang et al., 2015). Degradation kinetics, however, may be overestimated as they represent constant irradiation with light intensities of peak natural

312 daylight (CIE, 1989; QSun/QLab, 2011). Considering the mean annual solar surface
313 irradiation in northern Europe (100 – 200 W/m², accounting for e.g. diurnal and annual
314 variation) (Pfeifroth et al., 2018), photodegradation half-lives in the environment may
315 increase by one order of magnitude compared to half-lives estimated in the laboratory
316 experiments.

317 TerOH mainly formed during photodegradation under UV light, followed by
318 TerDesEOH. In contrast, TerSO and TerDesE concentrations initially increased and gradually
319 decreased during the experiment (Figure 1). Similar trends were observed during
320 photodegradation under artificial sunlight (Figure 1). For UV light induced transformation,
321 TerOH was formed either through substitution of the methylthio group by a hydroxy group
322 through hydroxy radicals, or through an oxidation of the methylthio group, leading to TerSO,
323 and further substitution of the oxidized methylthio group by a hydroxy group. This is
324 supported by an increase of TerSO concentrations, followed by TerSO depletion (Figure 1). A
325 similar pattern was observed for TerDesE formation through the loss of an ethyl group at the
326 side chain of terbutryn. TerDesEOH was likely formed through TerDesE by a cleavage of the
327 methylthio group and substitution through a hydroxy group. In contrast, the formation of
328 TerDesEOH through TerOH is unlikely as supported by constant TerOH concentrations up to
329 the end of the experiment. Desthiomethyl-terbutryn (TerDesS, Table S5) was previously
330 identified as a main TP formed through the loss of the -SCH_3 sidechain during
331 photodegradation under UV irradiation (Bollmann et al., 2016 and Hensen et al., 2018).
332 Although the contribution of TerDesS to the overall mass balance could not be quantified in
333 our experiment due to the lack of an analytical standard, it was likely limited as the mass
334 balance was nearly closed (>80 % recovery) with TerOH, TerDesEOH, TerSO and TerDesE.

335 The dominant TPs in photodegradation experiment with simulated sunlight were
336 TerDesEOH, TerOH, with lower and decreasing concentrations of TerDesE and TerSO at the

end of the experiment. TP patterns were similar in experiments with nitrate and distilled water. The dominance of terbutryn hydroxylation and/or dealkylation pathways suggest similar degradation patterns during direct and indirect photodegradation (Burrows et al., 2002; Hensen et al., 2019). However, on paint surfaces, TP formation patterns in photodegradation assays with UVB irradiation suggested a dependency on pigments and polymers that can get excited and cause indirect photodegradation (Urbanczyk et al., 2019). In pigment free paint, where most degradation occurred, TerSO increased before gradually decreasing, whereas TerDesEOH steadily increased, while TerOH concentrations reached a constant level (Urbanczyk et al., 2019). This latter pattern of TP formation is coherent with that of our study (Figure 1), highlighting the relevance to consider transformation processes on the facades.

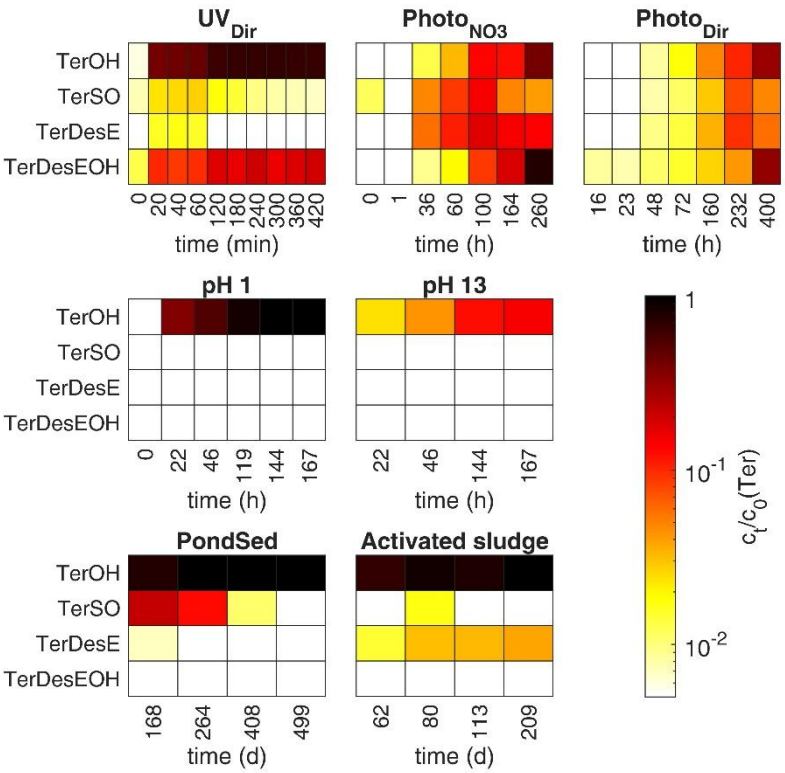

Figure 1. Transformation products formed during terbutryn photodegradation (top), abiotic hydrolysis (middle) and biodegradation (bottom). Results are given in molar concentrations normalized to the initial concentration of terbutryn (ter). No degradation was observed at pH

7. Transformation products in soil microcosms were only measured for one sampling (Figure S5).

Carbon and nitrogen stable isotope fractionations differed for photodegradation under UV light and with simulated sunlight but were similar for direct and indirect photodegradation under simulated sunlight. Photodegradation under UV light resulted in inverse isotope fractionation values, i.e., an enrichment of light isotopes in non-degraded fraction, for both carbon (ε_C = +0.8 ± 0.10 ‰) and nitrogen (ε_N = +2.2 ± 0.3). In contrast, simulated sunlight resulted in normal isotope fractionation (Table 1, Figure S6 and S7).

An inverse isotope effect for triazine transformation by UV light was related to excitation and relaxation processes or magnetic isotope effects (Drouin et al., 2021; Hartenbach et al., 2008; Knossow et al., 2020). An inverse isotope fractionation value during photodegradation under UV light was previously observed for atrazine, with a similar isotope fractionation value for nitrogen ($\varepsilon_{N(Atrazine)}$ = +2.4 ± 0.3 ‰) and more pronounced effect for carbon ($\varepsilon_{C(Atrazine)}$ = +2.7 ± 0.3 ‰) compared to isotope fractionation values for terbutryn degradation (Drouin et al., 2021; Hartenbach et al., 2008). A less pronounced carbon isotope fractionation during terbutryn degradation suggests terbutryn degradation to TerSO and then to TerOH, rather than the direct formation of TerOH. This idea is also supported by decreasing TerSO concentrations. The formation of TerSO may not significantly affect carbon or nitrogen isotope fractionation since carbon and nitrogen are not directly involved in bond cleavage or formation. In addition, constant TerOH concentrations indicate the formation of TerDesEOH through TerDesE rather than through TerOH. An inverse isotope fractionation may thus be caused by excitation at the triazine ring (Figure 2 A). The excitation may result in the formation of the singlet state and conversion to the triplet state with cleavage of the C-N

bond, e.g., during the formation of TerDesE. During the transition state, the bond is either cleaved or the molecule recombines. A recombination of the initial molecule is likelier for bonds containing light isotopes, resulting in enrichment of the light isotope in the non-degraded fraction. In addition, isotope fractionation may be more pronounced for nitrogen than for carbon, due to dilution effect for carbon isotopes.

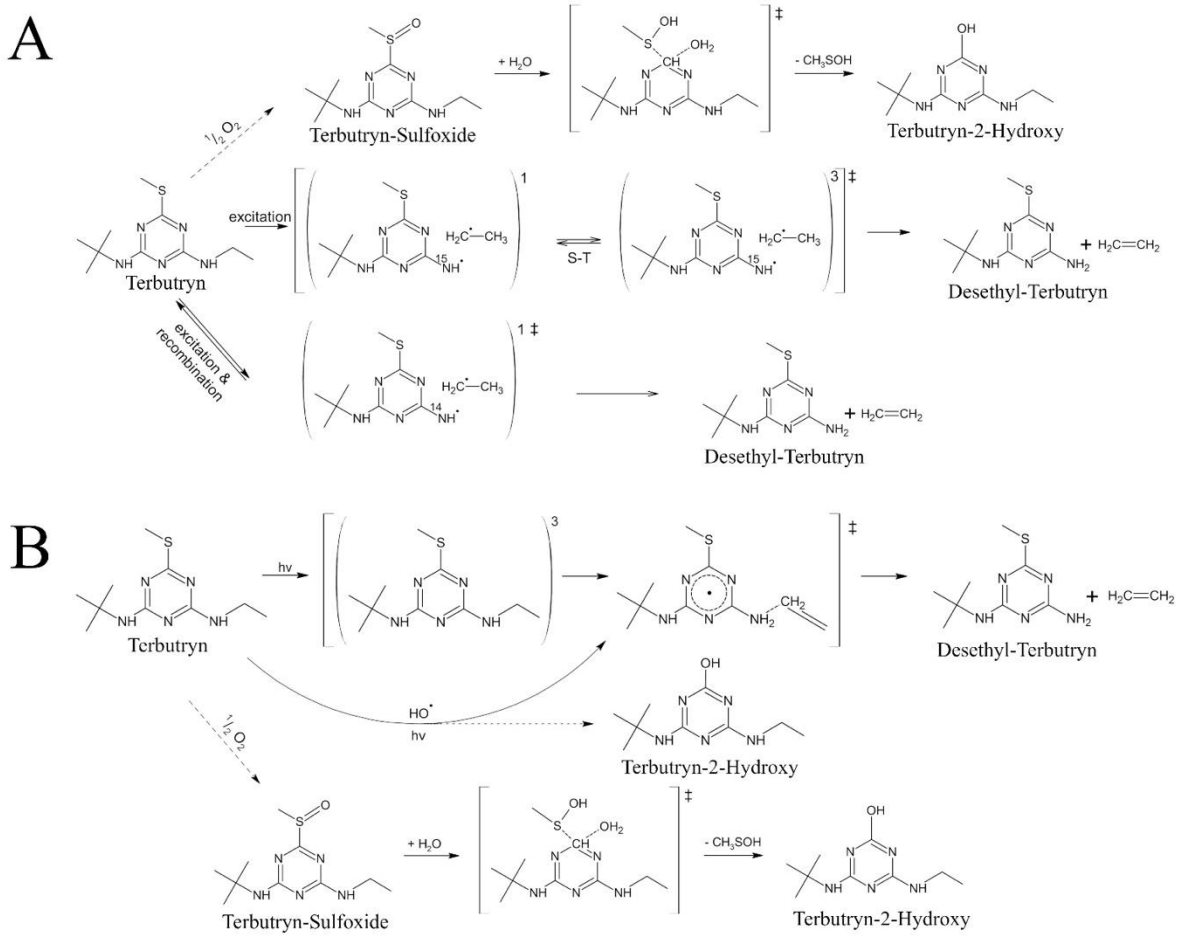

Figure 2. Suggested pathways for photodegradation of terbutryn under UV irradiation (λ = 254 nm) (A) and under simulated sunlight (B) modified from Knossow et al., 2020. Numbers at the brackets represent the singlet (1) or triplet (3) state of the molecule. The double-cross (‡) indicates the transition state. The dashed arrow in the reaction to TerSO implies that no Carbon or Nitrogen isotope fractionation is expected.

In contrast, simulated sunlight resulted in an enrichment of ^{13}C and ^{15}N in the non-degraded fraction of terbutryn in both direct (ε_C = –0.7 ± 0.3 ‰ and ε_N = –0.5 ± 0.3) and indirect (ε_C = –0.6 ± 0.2 ‰ and ε_N = –1.0 ± 0.4) experiments. Although several reactions may occur simultaneously during irradiation with sunlight, reaction mechanisms and associated isotope fractionation have been rarely examined. We hypothesize that degradation through TerSO to TerOH may occur under simulated sunlight with and without nitrate, causing insignificant carbon or nitrogen isotope fractionation as neither carbon nor nitrogen atoms are involved in bond cleavage. On the other hand, the formation of TerDesE and TerDesEOH suggests the excitation and the formation of a triplet state intermediate, which is further transformed into a terbutryn radical. The terbutryn radical might be delocalized over the aromatic ring as previously described for bromoxynil (Knossow et al., 2020), and weaken the C-N bond. This would result in bond cleavage during the formation of TerDesE through desethylation, causing normal isotope fractionation (Figure 2B). Worthy of note, the direct formation of TerOH in the presence of $OH^{\bullet}$ radicals (e.g., through excitation of nitrate) during indirect photodegradation cannot be excluded, however a deviation from isotope fractionation values of direct photodegradation would be expected.

3.2. Terbutryn hydrolysis

Overall, our results emphasize limited hydrolysis of terbutryn under most common environmental conditions. Terbutryn hydrolysis occurred at pH = 1 and pH = 13 but was insignificant at pH = 7 (Table 1). Acidic hydrolysis at pH = 1 was ten times faster than hydrolysis at pH = 13. Acidic hydrolysis occurs through bond cleavage catalyzed by H^+, whereas hydrolysis at pH 13 occurs through a base mediated reaction with OH^- as nucleophile (Wolfe et al., 1990).

411 Studies on hydrolysis of terbutryn are scarce, although previous studies on triazine
412 pesticides indicated high hydrolytic stability between pH = 5 and pH = 9 (Lewis et al., 2016;
413 Masbou et al., 2018), slow degradation at pH<4 and insignificant degradation at pH = 7 and
414 pH = 9 (Comber, 1999). While acidic rain (pH ~5; Keresztesi et al., 2019) may slightly
415 hydrolyze terbutryn in facade runoff, surface waters in Europe and Northern America
416 typically have higher pH values (Austnes et al., 2018). Alkaline pH values are rarely observed
417 in the environment but might occur, for example, in soda lakes (pH >10) (Grant and Sorokin,
418 2011) or directly in the pores of facade material (pH = 9.5) (Styszko et al., 2014). Overall, our
419 results indicate that the contribution of hydrolysis to the overall terbutryn degradation is
420 limited under typical environmental pH values and temperatures.

421 Only TerOH was detected during abiotic hydrolysis at pH = 1 and pH = 13, indicating
422 nucleophile substitution of the methylthio group under alkaline conditions (pH = 13) (Figure
423 3 A). Under acidic conditions, we hypothesize an intermediate step through the protonation of
424 the triazine ring followed by the cleavage of the SCH_3 group, as suggested for atrazine
425 (Meyer et al., 2009; Russell et al., 1968 Meyer et al., 2008), and in agreement with the
426 formation of TerOH during terbutryn acidic hydrolysis (Figure 3B).

427 Although TerOH was formed during both alkaline and acidic hydrolysis of terbutryn,
428 carbon and nitrogen isotope fractionation significantly differed, indicating distinct
429 degradation pathways (Table 1, Figure 1). Under alkaline hydrolysis, isotope fractionation
430 was observed for carbon ($\varepsilon_C = -1.3 \pm 0.2$), and to lesser extent for nitrogen ($\varepsilon_N = -0.4 \pm 0.3$).
431 The carbon isotope fractionation may be due to nucleophilic substitution of the methylthio
432 group during the formation of TerOH. The less pronounced nitrogen fractionation likely
433 results from a secondary isotope effect since no N atom is directly involved in the bond
434 cleavage (Figure 3 A). In contrast, acidic hydrolysis resulted in a normal isotope fractionation
435 for carbon ($\varepsilon_C = -3.4 \pm 0.7$) and an inverse isotope fractionation for nitrogen ($\varepsilon_N = +3.4 \pm 0.1$).

Protonation of a nitrogen atom in the triazine ring is leading to a polarization of the C-SCH_3 bond and the formation of TerOH (Figure 3 B). The bond cleavage at the methylthio group is expected to result in carbon isotope fractionation, as previously described for atrazine (Masbou et al., 2018; Meyer et al., 2009). Protonation of a nitrogen atom in the triazine ring would lead to an inverse isotope effect for nitrogen, as observed in this study. Such bonding is more stable for heavy isotopes in the transition state, resulting in an enrichment of light isotopes in the non-degraded fraction. Even though extreme pH values are unlikely to occur in the environment, slower degradation at less extreme pHs might result in similar TP formation and isotope fractionation since the reaction pathway is identical.

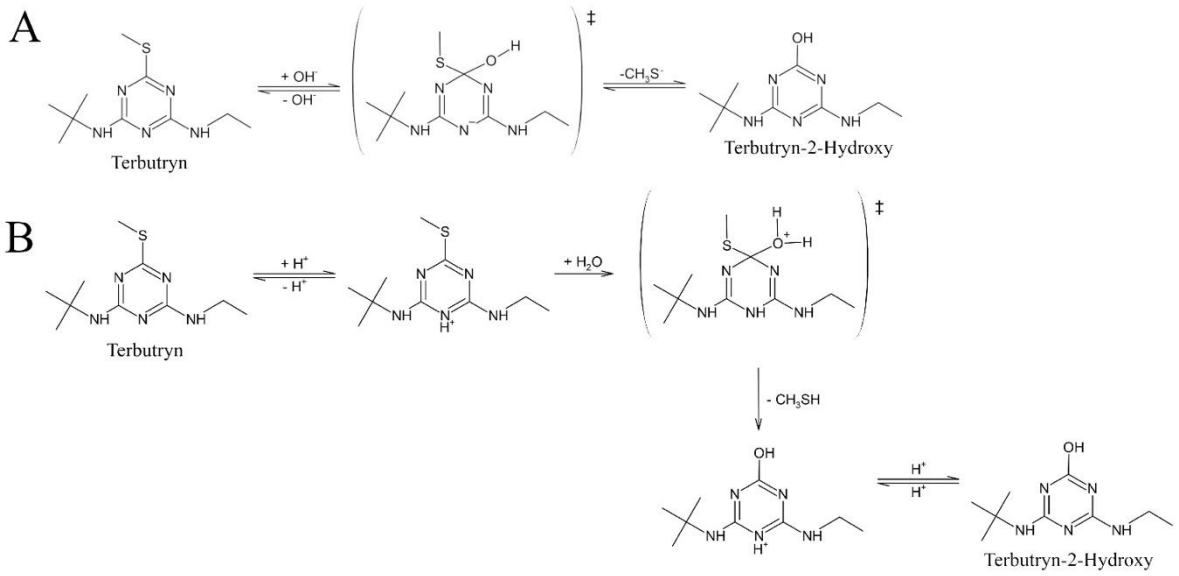

Figure 3. Suggested pathways of terbutryn transformation during abiotic hydrolysis at pH 13 (A) and pH 1 (B) (modified from Meyer et al., 2009). The double-cross (‡) indicates the transition state.

3.3. Terbutryn biodegradation

Half-lives for terbutryn biodegradation, ordered from the lowest to the highest half-lives: PondSed<Soil<activated sludge, were 4 to 62-fold higher than half-lives for terbutryn

photodegradation under simulated sunlight and hydrolysis (Table 1). However, biodegradation rates and sunlight induced degradation of terbutryn may be in the same order of magnitude since environmental photodegradation half-lives were overestimated in our study as previously discussed in section 3.1.

Overall, these results suggest slow terbutryn biodegradation in the environment. Microbial adaptation may explain faster terbutryn degradation in pond-sediment and soil experiments than in the activated sludge experiment (Poursat et al., 2019; Spain et al., 1980). Indeed, pond water and sediment in the PondSed, and soil in the soil experiments, were chronically exposed to direct release of terbutryn from facades at the sampling site. It is also worth noting that a wide range of half-lives (7 up to >240 days) for terbutryn degradation in previous laboratory studies underscores a strong dependency on the incubation method and matrix (Bollmann et al., 2017a; Lechón et al., 1997; Muir and Yarechewski, 1982). Half-lives for terbutryn degradation in activated WWTP sludge were two orders of magnitude higher than those in previous experiments with activated sewage sludge (2.1 to 7 days) (Luft et al., 2014). The initial amount and activity of degrading microorganisms in activated sewage inoculum may strongly vary among experiments, thereby affecting terbutryn degradation kinetics. In general, terbutryn degradation in WWTPs is expected to be limited as hydraulic retention times in WWTPs (<24 h) are typically lower than half-lives (Verlicchi et al., 2012). Terbutryn and other urban biocides were frequently detected in effluents and downstream of WWTPs, underlining the limited degradation in treatment facilities (Le et al., 2017; Paijens et al., 2021).

TerOH was the prevailing TP formed during biodegradation (Figure 1). TPs in soil microcosm experiments were only measured at one time point (Figure S5). We hypothesize that terbutryn degraded to TerSO, which was further degraded to TerOH (Luft et al., 2014). The degradation of methylthio-s-triazines through sulfoxides to the respective hydroxyl

derivates has been described previously (Kaufman and Kearney, 1976), and confirmed in degradation experiments with *Bacillus cereus* strain JUN7 (Harada et al., 2006). The prevalence of biodegradation via TerSO is also supported in our experiment by decreasing TerSO concentrations in sediment microcosms (PondSed), coinciding with increasing TerOH concentrations. A similar trend was observed in soil biodegradation experiments, alongside the formation of other TPs, including Desbutyl-2-hydroxy-terbutryn through a dealkylation of the TerOH sidechain (Bollmann et al., 2017a).

Terbutryn biodegradation did not lead to significant carbon and nitrogen stable isotope fractionation ($\Delta\delta^{13}C$ and $\Delta\delta^{15}N$ <0.5 ‰) (Table 1). This further supports the hypothesis of an initial terbutryn degradation to TerSO, although TerOH was the main TP detected during biodegradation. Indeed, the oxidation of the methylthio group to form TerSO could only lead to a secondary carbon or nitrogen isotope effect since carbon or nitrogen are not directly involved in bond cleavage (Figure 4). Further transformation from TerSO to TerOH is not affecting terbutryn stable isotope composition.

Altogether, both CSIA and TP data confirmed that degradation through the sulfoxide to the 2-hydroxy derivate is a major biodegradation pathway of terbutryn, in agreement with previous studies (Harada et al., 2006; Luft et al., 2014).

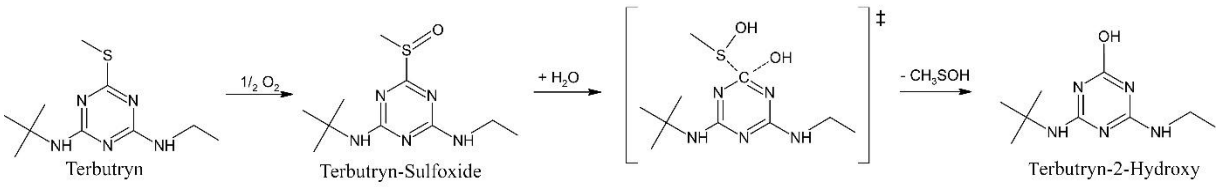

Figure 4. Suggested pathway of terbutryn biodegradation. The double-cross (‡) indicates the transition state.

3.4. Contribution of terbutryn degradation pathways in the environment

The dual carbon and nitrogen isotope plot shows that stable isotope fractionation patterns may help differentiate degradation pathways of terbutryn in the environment (Figure 5). This is relevant since classical concentration-based approaches cannot tease apart the contribution of sorption, dilution and degradation to the overall terbutryn dissipation. While single element CSIA provides a footprint of degradation when isotope values change due to kinetic isotope effect, distinct degradation pathways often occur simultaneously or consecutively, and thus may be mistaken. For instance, terbutryn direct photodegradation on facades may be followed by biodegradation in soil, and indirect photodegradation in a river or storm water retention pond.

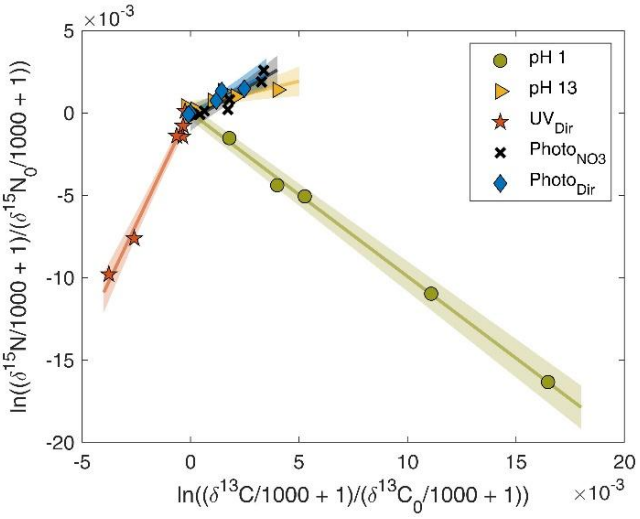

Figure 5. Dual C and N isotope plot for terbutryn degradation. Stable isotope fractionation patterns are represented at pH 1 (green circles), pH 13 (yellow triangles), irradiation with UV light (orange stars), irradiation under simulated sunlight in presence of nitrate (black crosses) and irradiation under simulated sunlight in pure water (blue diamonds). Shaded areas represent the 95 % confidence interval (CI) according to the York method (Ojeda et al., 2019). The origin (0,0) represents the original terbutryn isotope signature prior to degradation.

In this case, the dual element plot representing $\delta^{15}N$ against $\delta^{13}C$ values may help to identify degradation pathways of terbutryn. For instance, $\Lambda^{N/C}$ patterns for terbutryn photodegradation under UV light and with simulated sunlight indicate distinct transformation pathways (Figure 5). Hence, terbutryn photodegradation experiments under UV light have limited value to evaluate environmental photo-transformation because pathways differ from natural sunlight conditions but can be used to follow UV based remediation processes of water and wastewater (Yang et al., 2014). On the other hand, isotope fractionation patterns during direct and indirect terbutryn photodegradation are similar under simulated sunlight. This emphasizes that carbon and nitrogen stable isotope fractionation may help to distinguish terbutryn photodegradation from biodegradation or hydrolysis in environmental studies. However, the contribution of direct and indirect photodegradation may not be differentiated using carbon and nitrogen CSIA (Figure 5).

In addition, the direction and extent of isotope fractionation may indicate underlying reactions, reflecting degradation mechanisms, as shown for $^{15}N/^{14}N$ in terbutryn. Although TerOH is formed during both alkaline and acidic hydrolysis, the dual isotope plot highlights that the underlying degradation mechanisms differ substantially for abiotic acidic ($\Lambda^{N/C} = -1.0 \pm 0.1$) and alkaline ($\Lambda^{N/C} = 0.3 \pm 0.1$) hydrolysis of terbutryn (Figure 5). For instance, an unusual trend to more negative $\delta^{15}N$ values (inverse isotope effect) occurs during protonation of the nitrogen atoms during acidic hydrolysis as ^{15}N protonation is more stable than ^{14}N in the transition state. In contrast, the nucleophilic substitution of the methylthio group during alkaline hydrolysis of terbutryn results in normal isotope effect. This highlights the reaction specificity of multi element (ME) CSIA to identify degradation mechanisms, even when the same TP is eventually formed.

Altogether, combining TP analysis with carbon and nitrogen isotope CSIA allows to identify and compare pathways of terbutryn photodegradation under UV and simulated sunlight irradiation, abiotic acidic and alkaline hydrolysis and biodegradation (Figure 6).

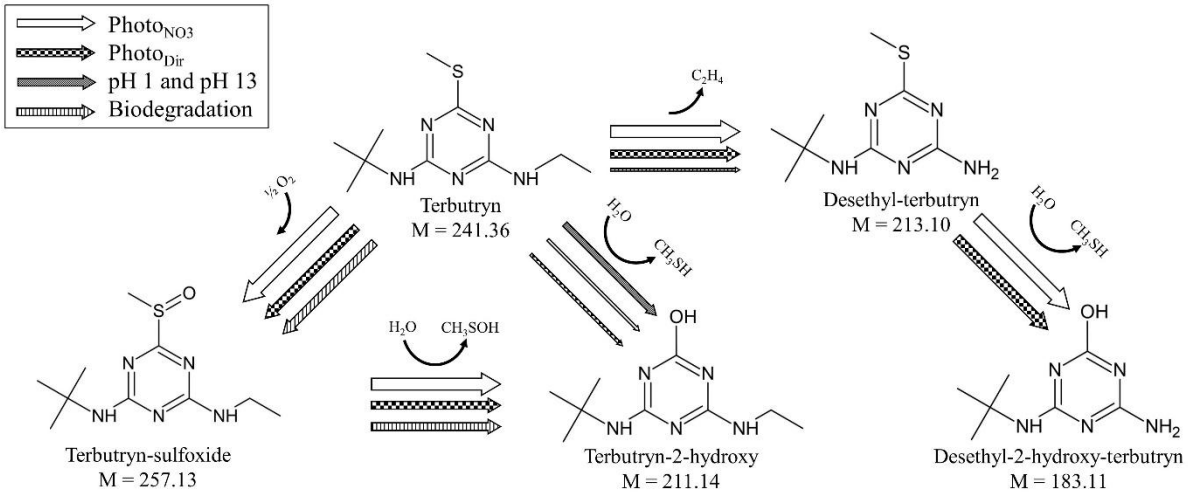

Figure 6. Putative degradation pathways of terbutryn in the environment. The thickness of the arrows indicates the contribution of each process to the overall degradation. Thick arrows indicate the main contribution while thinner arrows indicate minor contribution of the respective degradation pathway to the overall terbutryn transformation.

Conclusion

Better knowledge of degradation kinetics and pathways of terbutryn in different environmental compartments may help to evaluate the terbutryn reactive transport across the facade-soil-water continuum. Our results emphasize that photodegradation may contribute to terbutryn degradation on the facade and in waters. Since setups and irradiation intensities of simulated sunlight experiments require correction for the local irradiation intensities, degradation rates indicate further terbutryn accumulation in the environment. Terbutryn released from facades during rainfall events may accumulate in soil receiving facade wash-off due to limited terbutryn biodegradation and hydrolysis. In particular, the contribution of

559 abiotic hydrolysis to terbutryn degradation appears negligible under most environmental
560 conditions.

561 Most importantly, the combination of ME-CSIA data and TP quantification allowed to
562 identify and tease apart degradation pathways of terbutryn. While terbutryn TPs help to
563 identify degradation pathways, distinct degradation pathways may lead to the same TPs,
564 thereby limiting the interpretation. Our results highlight that terbutryn CSIA can help
565 identifying underlying degradation pathways based on a dual isotope approach and
566 differentiate pathways *in situ*, even without TP measurements. Isotope fractionation patterns
567 during direct and indirect terbutryn photodegradation under simulated sunlight are similar,
568 while terbutryn biodegradation does not lead to significant isotope fractionation. Hence,
569 carbon and nitrogen stable isotope fractionation may help to distinguish terbutryn
570 photodegradation from biodegradation in environmental studies.

571 In the future, insights into degradation pathways from ME-CSIA may be gained with
572 sulphur stable isotope fractionation ($\delta^{34}S$) during terbutryn degradation based on GC-MS-
573 ICPMS measurements (Kümmel et al., 2020; Torrentó et al., 2021). Sulphur stable isotope
574 values may significantly change during biodegradation through the formation of TerSO, while
575 the formation of a bond between the sulphur and oxygen atoms may cause an inverse isotope
576 effect (i.e., more negative $\delta^{34}S$ values) (Figure 4). It is thus expected that sulphur stable
577 isotope fractionation may help teasing apart biodegradation and photodegradation during
578 terbutryn leaching from the facade up to groundwater.

579 Altogether, we anticipate our study to be a starting point for a new strategy including
580 ME-CSIA to examine terbutryn transformation on facades and in receiving environmental
581 compartments to follow up mitigation measures to limit biocide release.

582

Acknowledgements

This research was funded by the EU within the European Regional Development Fund (ERDF), support measure INTERREG V in the Upper Rhine as part of the NAVEBGO project 5.3 (sustainable reduction of biocide inputs to groundwater in the Upper Rhine region). The authors acknowledge Benoit Guyot for support in method development on the LC-MS/MS, Anna Messang and Jean-Baptiste Josselin for support in photodegradation experiments and Jérémy Masbou and Lena Schnarr for useful discussion and comments. Elemental and isotopic analyses were performed at the Pacite platform of University of Strasbourg at ITES (Strasbourg – France).

Author contribution statement

Tobias Junginger: Conceptualization; Data curation; Formal analysis; Investigation; Methodology; Visualization; Writing – original draft. **Sylvain Payraudeau**: Formal analysis; Project administration; Resources; Software; Supervision; Validation; Writing – review & editing. **Gwenaël Imfeld:** Conceptualization; Data curation; Formal analysis; Funding acquisition; Methodology; Project administration; Resources; Supervision; Validation; Visualization; Writing – review & editing.

References

Alvarez-Zaldívar, P., Payraudeau, S., Meite, F., Masbou, J., Imfeld, G., 2018. Pesticide degradation and export losses at the catchment scale: insights from compound-specific isotope analysis (CSIA). Water Res. 139, 198–207. https://doi.org/10.1016/j.watres.2018.03.061

Austnes, K., Aherne, J., Arle, J., Čičendajeva, M., Couture, S., Fölster, J., Garmo, Ø.A., Hruska, J., Monteith, D., Posch, M., Rogora, M., Sample, J.E., Skjelkvåle, B.L., Steingruber, S., Stoddard, J.L., Ulańczyk, R., Van Dam, H., Velasco, M.T., Vuorenmaa, J., Wright, R.F., de Wit, H., 2018. Regional assessment of the current extent of acidification of surface waters in Europe and North America, 134. Norwegian institute for water research.

Bollmann, U.E., Fernández-Calviño, D., Brandt, K.K., Storgaard, M.S., Sanderson, H., Bester, K., 2017a. Biocide runoff from building facades: degradation kinetics in soil. Environ. Sci. Technol. 51, 3694–3702. https://doi.org/10.1021/acs.est.6b05512

Bollmann, U.E., Minelgaite, G., Schlüsener, M., Ternes, T., Vollertsen, J., Bester, K., 2016. Leaching of terbutryn and its photodegradation products from artificial walls under natural weather conditions. Environ. Sci. Technol. 50, 4289–4295. https://doi.org/10.1021/acs.est.5b05825

Bollmann, U.E., Minelgaite, G., Schlüsener, M., Ternes, T.A., Vollertsen, J., Bester, K., 2017b. Photodegradation of octylisothiazolinone and semi-field emissions from facade coatings. Sci. Rep. 7, 41501. https://doi.org/10.1038/srep41501

Burkhardt, M., Junghans, M., Zuleeg, S., Boller, M., Schoknecht, U., Lamani, X., Bester, K., Vonbank, R., Simmler, H., 2009. Biozide in Gebäudefassaden – ökotoxikologische Effekte, Auswaschung und Belastungsabschätzung für Gewässer. Environ. Sci. Eur. 21, 36–47. https://doi.org/10.1007/s12302-008-0033-1

630 Burkhardt, M., Zuleeg, S., Vonbank, R., Bester, K., Carmeliet, J., Boller, M., Wangler, T., 2012.
631 Leaching of biocides from façades under natural weather conditions. Environ. Sci. Technol. 46,
632 5497–5503. https://doi.org/10.1021/es2040009
633 Burrows, H.D., Canle L, M., Santaballa, J.A., Steenken, S., 2002. Reaction pathways and mechanisms
634 of photodegradation of pesticides. J. Photochem. Photobiol. B: Biol. 67, 71–108.
635 https://doi.org/10.1016/S1011-1344(02)00277-4
636 Carazo-Rojas, E., Pérez-Rojas, G., Pérez-Villanueva, M., Chinchilla-Soto, C., Chin-Pampillo, J.S., Aguilar-
637 Mora, P., Alpízar-Marín, M., Masís-Mora, M., Rodríguez-Rodríguez, C.E., Vryzas, Z., 2018. Pesticide
638 monitoring and ecotoxicological risk assessment in surface water bodies and sediments of a
639 tropical agro-ecosystem. Environ. Pollut. 241, 800–809.
640 https://doi.org/10.1016/j.envpol.2018.06.020
641 Ccanccapa, A., Masiá, A., Navarro-Ortega, A., Picó, Y., Barceló, D., 2016. Pesticides in the Ebro river
642 basin: occurrence and risk assessment. Environ. Pollut. 211, 414–424.
643 https://doi.org/10.1016/j.envpol.2015.12.059
644 CIE, 1989. CIE 85 - Solar Spectral Irradiance (1st Edition) (E) | Engineering360, International
645 Comission on Illumination (CIE).
646 Comber, S.D.W., 1999. Abiotic persistence of atrazine and simazine in water. Pesticide Science 55,
647 696–702. https://doi.org/10.1002/(SICI)1096-9063(199907)55:7<696::AID-PS11>3.0.CO;2-7
648 Coplen, T.B., 2011. Guidelines and recommended terms for expression of stable-isotope-ratio and
649 gas-ratio measurement results. Rapid Commun. Mass Spectrom. 25, 2538–2560.
650 https://doi.org/10.1002/rcm.5129
651 Drouin, G., Droz, B., Leresche, F., Payraudeau, S., Masbou, J., Imfeld, G., 2021. Direct and indirect
652 photodegradation of atrazine and S-metolachlor in agriculturally impacted surface water and
653 associated C and N isotope fractionation. Environ. Sci.: Processes Impacts 23, 1791–1802.
654 https://doi.org/10.1039/D1EM00246E

Droz, B., Drouin, G., Maurer, L., Villette, C., Payraudeau, S., Imfeld, G., 2021. Phase transfer and biodegradation of pesticides in water–sediment systems explored by compound-specific isotope analysis and conceptual modeling. Environ. Sci. Technol. 55, 4720–4728. https://doi.org/10.1021/acs.est.0c06283

Elsner, M., 2010. Stable isotope fractionation to investigate natural transformation mechanisms of organic contaminants: principles, prospects and limitations. J. Environ. Monit. 12, 2005–2031. https://doi.org/10.1039/C0EM00277A

Elsner, M., Imfeld, G., 2016. Compound-specific isotope analysis (CSIA) of micropollutants in the environment — current developments and future challenges. Curr. Opin. Biotechnol., Analytical biotechnology 41, 60–72. https://doi.org/10.1016/j.copbio.2016.04.014

Elsner, M., Jochmann, M.A., Hofstetter, T.B., Hunkeler, D., Bernstein, A., Schmidt, T.C., Schimmelmann, A., 2012. Current challenges in compound-specific stable isotope analysis of environmental organic contaminants. Anal. Bioanal. Chem. 403, 2471–2491. https://doi.org/10.1007/s00216-011-5683-y

European Council Directive 91/414/EEC, 2002. Commission Regulation (EC) No 2076/2002 of 20 November 2002 extending the time period referred to in Article 8(2) of Council Directive 91/414/EEC and concerning the non-inclusion of certain active substances in Annex I to that Directive and the withdrawal of authorisations for plant protection products containing these substances (Text with EEA relevance), OJ L.

European Council Directive 2013/39/EU, 2013. Directive 2013/39/EU of the European Parliament and of the Council of 12 August 2013 amending Directives 2000/60/EC and 2008/105/EC as regards priority substances in the field of water policy Text with EEA relevance, OJ L.

Fenner, K., Canonica, S., Wackett, L.P., Elsner, M., 2013. Evaluating pesticide degradation in the environment: blind spots and emerging opportunities. Science. https://doi.org/10.1126/science.1236281

680 Fischer, A., Manefield, M., Bombach, P., 2016. Application of stable isotope tools for evaluating
681 natural and stimulated biodegradation of organic pollutants in field studies. Curr. Opin.
682 Biotechnol. 41, 99–107. https://doi.org/10.1016/j.copbio.2016.04.026
683 Grant, W.D., Sorokin, D.Yu., 2011. Distribution and diversity of soda lake alkaliphiles, in: Horikoshi, K.
684 (Ed.), Extremophiles Handbook. Springer Japan, Tokyo, pp. 27–54. https://doi.org/10.1007/978-4-
685 431-53898-1_3
686 Harada, N., Takagi, K., Fujii, K., Iwasaki, A., 2006. Transformation of methylthio-s-triazines via sulfur
687 oxidation by strain JUN7, a Bacillus cereus species. Soil Biol. Biochem. 38, 2952–2957.
688 https://doi.org/10.1016/j.soilbio.2006.03.018
689 Hartenbach, A.E., Hofstetter, T.B., Tentscher, P.R., Canonica, S., Berg, M., Schwarzenbach, R.P., 2008.
690 Carbon, hydrogen, and nitrogen isotope fractionation during light-induced transformations of
691 atrazine. Environ. Sci. Technol. 42, 7751–7756. https://doi.org/10.1021/es800356h
692 Hensen, B., Lange, J., Jackisch, N., Zieger, F., Olsson, O., Kümmerer, K., 2018. Entry of biocides and
693 their transformation products into groundwater via urban stormwater infiltration systems. Water
694 Res. 144, 413–423. https://doi.org/10.1016/j.watres.2018.07.046
695 Hensen, B., Olsson, O., Kümmerer, K., 2019. The role of irradiation source setups and indirect
696 phototransformation: kinetic aspects and the formation of transformation products of weakly
697 sunlight-absorbing pesticides. Sci. Total Environ. 695, 133808.
698 https://doi.org/10.1016/j.scitotenv.2019.133808
699 Hoefs, J., 2015. Stable isotope geochemistry. Springer International Publishing, Cham.
700 https://doi.org/10.1007/978-3-319-19716-6
701 Höhener, P., Imfeld, G., 2021. Quantification of Lambda (Λ) in multi-elemental compound-specific
702 isotope analysis. Chemosphere 267. https://doi.org/10.1016/j.chemosphere.2020.129232
703 Höhener, P., Yu, X., 2012. Stable carbon and hydrogen isotope fractionation of dissolved organic
704 groundwater pollutants by equilibrium sorption. J. Contam. Hydrol. 129–130, 54–61.
705 https://doi.org/10.1016/j.jconhyd.2011.09.006

706 Ivdra, N., Herrero-Martín, S., Fischer, A., 2014. Validation of user- and environmentally friendly
707 extraction and clean-up methods for compound-specific stable carbon isotope analysis of
708 organochlorine pesticides and their metabolites in soils. J. Chromatogr. A 1355, 36–45.
709 https://doi.org/10.1016/j.chroma.2014.06.014
710 Jungnickel, C., Stock, F., Brandsch, T., Ranke, J., 2008. Risk assessment of biocides in roof paint. Part
711 1: experimental determination and modelling of biocide leaching from roof paint. Environ. Sci.
712 Pollut. Res. Int. 15, 258–265. https://doi.org/10.1065/espr2007.12.465
713 Jurado, A., Fernandes, M., Videira, R., Peixoto, F., Vicente, J., 2011. Herbicides: the face and the
714 reverse of the coin. An in vitro approach to the toxicity of herbicides in non-target organisms,
715 Herbicides and Environment. IntechOpen. https://doi.org/10.5772/12976
716 Kaufman, D.D., Kearney, P.C., 1976. Microbial transformations in the soil. Herbicides: Physiology.
717 Keresztesi, Á., Birsan, M.-V., Nita, I.-A., Bodor, Z., Szép, R., 2019. Assessing the neutralisation, wet
718 deposition and source contributions of the precipitation chemistry over Europe during 2000–
719 2017. Environ. Sci. Eur. 31, 50. https://doi.org/10.1186/s12302-019-0234-9
720 Knossow, N., Siebner, H., Bernstein, A., 2020. Isotope analysis method for the herbicide bromoxynil
721 and its application to study photo-degradation processes. J. Hazard. Mater. 388, 122036.
722 https://doi.org/10.1016/j.jhazmat.2020.122036
723 Kresmann, S., Arokia, A.H.R., Koch, C., Sures, B., 2018. Ecotoxicological potential of the biocides
724 terbutryn, octhilinone and methylisothiazolinone: underestimated risk from biocidal pathways?
725 Sci. Total Environ. 625, 900–908. https://doi.org/10.1016/j.scitotenv.2017.12.280
726 Kümmel, S., Horst, A., Gelman, F., Strauss, H., Richnow, H.H., Gehre, M., 2020. Simultaneous
727 compound-specific analysis of $\delta^{33}S$ and $\delta^{34}S$ in organic compounds by GC-MC-ICPMS using
728 medium- and low-mass-resolution modes. Anal. Chem. 92, 14685–14692.
729 https://doi.org/10.1021/acs.analchem.0c03253

730 Lam, M.W., Tantuco, K., Mabury, S.A., 2003. PhotoFate: a new approach in accounting for the
731 contribution of indirect photolysis of pesticides and pharmaceuticals in purface waters. Environ.
732 Sci. Technol. 37, 899–907. https://doi.org/10.1021/es025902+
733 Le, T.D.H., Scharmüller, A., Kattwinkel, M., Kühne, R., Schüürmann, G., Schäfer, R.B., 2017.
734 Contribution of waste water treatment plants to pesticide toxicity in agriculture catchments.
735 Ecotoxicol. Environ. Saf. 145, 135–141. https://doi.org/10.1016/j.ecoenv.2017.07.027
736 LeBaron, H.M., McFarland, J.E., Burnside, O., 2008. The triazine herbicides: 50 years revolutionizing
737 agriculture. Elsevier.
738 Lechón, Y., Sánchez-Brunete, C., Tadeo, J.L., 1997. Influence of the laboratory incubation method on
739 chlorotoluron and terbutryn degradation in soil. J. Agric. Food Chem. 45, 951–954.
740 https://doi.org/10.1021/jf960340x
741 Lewis, K.A., Tzilivakis, J., Warner, D.J., Green, A., 2016. An international database for pesticide risk
742 assessments and management. Hum. Ecol. Risk Assess. 22, 1050–1064.
743 https://doi.org/10.1080/10807039.2015.1133242
744 Lihl, C., Heckel, B., Grzybkowska, A., Dybala-Defratyka, A., Ponsin, V., Torrentó, C., Hunkeler, D.,
745 Elsner, M., 2020. Compound-specific chlorine isotope fractionation in biodegradation of atrazine.
746 Environ. Sci.: Processes Impacts 22, 792–801. https://doi.org/10.1039/C9EM00503J
747 Linke, F., Olsson, O., Preusser, F., Kümmerer, K., Schnarr, L., Bork, M., Lange, J., 2021. Sources and
748 pathways of biocides and their transformation products in urban storm water infrastructure of a 2
749 ha urban district. Hydrol. Earth Syst. Sci. 25, 4495–4512. https://doi.org/10.5194/hess-25-4495-
750 2021
751 Luft, A., Wagner, M., Ternes, T.A., 2014. Transformation of biocides irgarol and terbutryn in the
752 biological wastewater treatment. Environ. Sci. Technol. 48, 244–254.
753 https://doi.org/10.1021/es403531d
754 Mabey, W., Mill, T., 1978. Critical review of hydrolysis of organic compounds in water under
755 environmental conditions. J. Phys. Chem. Ref. Data 7, 383–415. https://doi.org/10.1063/1.555572

Machate, O., Dellen, J., Schulze, T., Wentzky, V.C., Krauss, M., Brack, W., 2021. Evidence for antifouling biocides as one of the limiting factors for the recovery of macrophyte communities in lakes of Schleswig-Holstein. Environ. Sci. Eur. 33, 57. https://doi.org/10.1186/s12302-021-00500-3

Masbou, J., Drouin, G., Payraudeau, S., Imfeld, G., 2018. Carbon and nitrogen stable isotope fractionation during abiotic hydrolysis of pesticides. Chemosphere 213, 368–376. https://doi.org/10.1016/j.chemosphere.2018.09.056

Meyer, A.H., Penning, H., Elsner, M., 2009. C and N isotope fractionation suggests similar mechanisms of microbial atrazine transformation despite involvement of different enzymes (AtzA and TrzN). Environ. Sci. Technol. 43, 8079–8085. https://doi.org/10.1021/es9013618

Minelgaite, G., Nielsen, A.H., Pedersen, M.L., Vollertsen, J., 2017. Photodegradation of three stormwater biocides. Urban Water J. 14, 53–60. https://doi.org/10.1080/1573062X.2015.1076489

Muir, D.C., Yarechewski, A.L., 1982. Degradation of terbutryn in sediments and water under various redox conditions. J. Environ. Sci. Health - B Pestic. Food Contam. Agric. Wastes 17, 363–380. https://doi.org/10.1080/03601238209372327

Ojeda, A.S., Phillips, E., Mancini, S.A., Lollar, B.S., 2019. Sources of uncertainty in biotransformation mechanistic interpretations and remediation studies using CSIA. Anal. Chem. 91, 9147–9153. https://doi.org/10.1021/acs.analchem.9b01756

Paijens, C., Bressy, A., Frère, B., Tedoldi, D., Mailler, R., Rocher, V., Neveu, P., Moilleron, R., 2021. Urban pathways of biocides towards surface waters during dry and wet weathers: assessment at the Paris conurbation scale. J. Hazard. Mater. 402, 123765. https://doi.org/10.1016/j.jhazmat.2020.123765

Pfeifroth, U., Sanchez-Lorenzo, A., Manara, V., Trentmann, J., Hollmann, R., 2018. Trends and variability of surface solar radiation in Europe based on surface- and satellite-based data records. J. Geophys. Res. Atmos. 123, 1735–1754. https://doi.org/10.1002/2017JD027418

780 Poursat, B.A.J., van Spanning, R.J.M., de Voogt, P., Parsons, J.R., 2019. Implications of microbial
781 adaptation for the assessment of environmental persistence of chemicals. Crit. Rev. Environ. Sci.
782 Technol. 49, 2220–2255. https://doi.org/10.1080/10643389.2019.1607687
783 QSun/QLab, 2011. Q-Lab QSun Technical bulletin LU-0822: sunlight, weathering & light stability
784 testing [WWW Document]. URL https://www.q-lab.com/documents/public/cd131122-c252-4142-
785 86ce-5ba366a12759.pdf (accessed 2.9.22).
786 Quednow, K., Püttmann, W., 2007. Monitoring terbutryn pollution in small rivers of Hesse, Germany.
787 J. Environ. Monit. 9, 1337–1343. https://doi.org/10.1039/B711854F
788 Russell, J.D., Cruz, M., White, J.L., Bailey, G.W., W. R. Payne, J., J. D. Pope, J., Teasley, J.I., 1968. Mode
789 of chemical degradation of s-triazines by montmorillonite. Science.
790 https://doi.org/10.1126/science.160.3834.1340
791 Sakkas, V.A., Konstantinou, I.K., Albanis, T.A., 2006. Photochemical fate of organic booster biocides in
792 the aquatic environment, in: Konstantinou, I.K. (Ed.), Antifouling Paint Biocides, The Handbook of
793 Environmental Chemistry. Springer, Berlin, Heidelberg, pp. 171–200.
794 https://doi.org/10.1007/698_5_054
795 Schmidt, T.C., Zwank, L., Elsner, M., Berg, M., Meckenstock, R.U., Haderlein, S.B., 2004. Compound-
796 specific stable isotope analysis of organic contaminants in natural environments: a critical review
797 of the state of the art, prospects, and future challenges. Anal. Bioanal. Chem. 378, 283–300.
798 https://doi.org/10.1007/s00216-003-2350-y
799 Schoknecht, U., Gruycheva, J., Mathies, H., Bergmann, H., Burkhardt, M., 2009. Leaching of biocides
800 used in façade coatings under laboratory test conditions. Environ. Sci. Technol. 43, 9321–9328.
801 https://doi.org/10.1021/es9019832
802 Schoknecht, U., Mathies, H., Lisec, J., 2021. Leaching and transformation of film preservatives in
803 paints induced by combined exposure to ultraviolet radiation and water contact under controlled
804 laboratory conditions. Water 13, 2390. https://doi.org/10.3390/w13172390

805 Schürner, H.K.V., Seffernick, J.L., Grzybkowska, A., Dybala-Defratyka, A., Wackett, L.P., Elsner, M.,
806 2015. Characteristic isotope fractionation patterns in s-triazine degradation have their origin in
807 multiple protonation options in the s-triazine hydrolase TrzN. Environ. Sci. Technol. 49, 3490–
808 3498. https://doi.org/10.1021/es5055385
809 Schüth, C., Taubald, H., Bolaño, N., Maciejczyk, K., 2003. Carbon and hydrogen isotope effects during
810 sorption of organic contaminants on carbonaceous materials. J. Contam. Hydrol. 64, 269–281.
811 https://doi.org/10.1016/S0169-7722(02)00216-4
812 Schwarzenbach, R.P., Gschwend, P.M., Imboden, D.M., 2005. Environmental organic chemistry. John
813 Wiley & Sons.
814 Scott, K.M., Lu, X., Cavanaugh, C.M., Liu, J.S., 2004. Optimal methods for estimating kinetic isotope
815 effects from different forms of the Rayleigh distillation equation. Geochim. Cosmochim. Acta 68,
816 433–442. https://doi.org/10.1016/S0016-7037(03)00459-9
817 Spain, J.C., Pritchard, P.H., Bourquin, A.W., 1980. Effects of adaptation on biodegradation rates in
818 sediment/water cores from estuarine and freshwater environments. Appl. Environ. Microbiol. 40,
819 726–734. https://doi.org/10.1128/aem.40.4.726-734.1980
820 Styszko, K., Bollmann, U.E., Bester, K., 2015. Leaching of biocides from polymer renders under
821 wet/dry cycles--rates and mechanisms. Chemosphere 138, 609–615.
822 https://doi.org/10.1016/j.chemosphere.2015.07.029
823 Styszko, K., Bollmann, U.E., Wangler, T.P., Bester, K., 2014. Desorption of biocides from renders
824 modified with acrylate and silicone. Chemosphere 95, 188–192.
825 https://doi.org/10.1016/j.chemosphere.2013.08.064
826 Talja, K.M., Kaukonen, S., Kilpi-Koski, J., Malin, I., Kairesalo, T., Romantschuk, M., Tuominen, J.,
827 Kontro, M.H., 2008. Atrazine and terbutryn degradation in deposits from groundwater
828 environment within the boreal region in Lahti, Finland. J. Agric. Food Chem. 56, 11962–11968.
829 https://doi.org/10.1021/jf802528a

Torabi, E., Wiegert, C., Guyot, B., Vuilleumier, S., Imfeld, G., 2020. Dissipation of S-metolachlor and butachlor in agricultural soils and responses of bacterial communities: insights from compound-specific isotope and biomolecular analyses. J. Environ. Sci. 92, 163–175. https://doi.org/10.1016/j.jes.2020.02.009

Torrentó, C., Ponsin, V., Lihl, C., Hofstetter, T.B., Baran, N., Elsner, M., Hunkeler, D., 2021. Triple-element compound-specific stable isotope analysis (3D-CSIA): added value of Cl isotope ratios to assess herbicide degradation. Environ. Sci. Technol. 55, 13891–13901. https://doi.org/10.1021/acs.est.1c03981

Urbanczyk, M.M., Bester, K., Borho, N., Schoknecht, U., Bollmann, U.E., 2019. Influence of pigments on phototransformation of biocides in paints. J. Hazard. Mater. 364, 125–133. https://doi.org/10.1016/j.jhazmat.2018.10.018

Verlicchi, P., Al Aukidy, M., Zambello, E., 2012. Occurrence of pharmaceutical compounds in urban wastewater: removal, mass load and environmental risk after a secondary treatment—a review. Sci. Total Environ. 429, 123–155. https://doi.org/10.1016/j.scitotenv.2012.04.028

Vermeesch, P., 2018. IsoplotR: a free and open toolbox for geochronology. Geosci. Front. 9, 1479–1493. https://doi.org/10.1016/j.gsf.2018.04.001

Wittmer, I.K., Scheidegger, R., Bader, H.-P., Singer, H., Stamm, C., 2011. Loss rates of urban biocides can exceed those of agricultural pesticides. Sci. Total Environ. 409, 920–932. https://doi.org/10.1016/j.scitotenv.2010.11.031

Wolfe, N.L., Mingelgrin, U., Miller, G.C., 1990. Abiotic transformations in water, sediments, and soil, in: Pesticides in the Soil Environment: Processes, Impacts and Modeling. John Wiley & Sons, Ltd, pp. 103–168. https://doi.org/10.2136/sssabookser2.c5

Wu, B., Arnold, W.A., Ma, L., 2021. Photolysis of atrazine: role of triplet dissolved organic matter and limitations of sensitizers and quenchers. Water Research 190, 116659. https://doi.org/10.1016/j.watres.2020.116659

855 Yang, W., Zhou, H., Cicek, N., 2014. Treatment of organic micropollutants in water and wastewater by
856 UV-based processes: a literature review. Crit. Rev. Environ. Sci. Technol. 44, 1443–1476.
857 https://doi.org/10.1080/10643389.2013.790745
858 Zhang, N., Schindelka, J., Herrmann, H., George, C., Rosell, M., Herrero-Martín, S., Klán, P., Richnow,
859 H.H., 2015. Investigation of humic substance photosensitized reactions via carbon and hydrogen
860 isotope fractionation. Environ. Sci. Technol. 49, 233–242. https://doi.org/10.1021/es502791f
861